JOURNAL OF MATERIALS SCIENCE 12 (1977) 893–903

The direct observation and analysis of dislocations in experimentally deformed plagioclase feldspars

D. B. MARSHALL, A. C. McLAREN
Department of Physics, Monash University, Clayton, Victoria, Australia

Transmission electron microscopy has been used to observe and analyse the dislocations in a series of plagioclase feldspars which had been experimentally deformed in compression. The results indicate that a moving dislocation in these materials leaves behind a fault in the structure. Two types of fault are observed but both define the slip plane of the associated dislocation. From these observations, together with stuctural considerations, the visibility of the dislocations and the orientatation of the applied shear stress it has been possible to determine the slip system uniquely for a number of dislocations. The origin of the dislocations and the nature of the faults are also discussed.

1. Introduction

The plagioclase feldspars form one of the most important groups of rock-forming minerals. Although they are strong and brittle under normal conditions of temperature and pressure, there is abundant geological evidence for their ductility. When they are experimentally deformed in triaxial compression, intragranular flow is observed only at high temperatures and pressures. Borg and Heard [1, 2] found that for strain-rates of $2 \times 10^{-5}\,\text{sec}^{-1}$ ductile deformation was mainly absent for confining pressures of 5 kbar and temperatures ranging up to 700° C. However, their optical observations indicate that, at confining pressures of 8 to 10 kbar and at temperatures of 800° C, faulting and cataclassis (local fracture) are much suppressed and mechanical twinning and (0 1 0) slip (as deduced from the geometry of kink bands) become common.

More recently, electron microscope observations have been made of the substructures in naturally deformed plagioclase. Lorimer *et al.* [3, 4] described dislocation cell-structures characteristic of recovery in naturally deformed sodic (sodium-rich) plagioclases. White [5] and Marshall and Wilson [6] described the deformation substructures and recrystallization of naturally deformed sodic plagioclases and Lally *et al.* [7] found evidence of recovery and recrystallization in lunar plagioclase.

The present investigation involves the use of transmission electron microscopy for the direct observation and identification of the crystal defects responsible for the ductility of a series of experimentally deformed plagioclases. Deformation takes place by three main mechanisms: (1) brittle fracture, mostly along cleavage planes; (2) mechanical albite and pericline twinning; and (3) slip due to the generation and motion of dislocations. In addition, "micro-shear bands" are produced, but they contribute very little to the total strain and therefore will be discussed elsewhere. This paper is concerned only with the detailed nature of the dislocations and identification of their slip systems. An important observation is that a moving dislocation always appears to generate a strip of fault which defines the slip plane. From this and other structural considerations, it has been possible to determine the slip systems uniquely for many dislocations.

2. Structural considerations

The feldspar structure is based on a framework of TO_4 (T = Si, Al) tetrahedra, where the O atoms of the framework form irregularly shaped cavities which are occupied by Na, K or Ca cations [8]. The plagioclase feldspars form the mineral series from albite ($NaAlSi_3O_8$) to anorthite ($CaAl_2Si_2O_8$)

and they are all triclinic except for the high temperature form of albite (monalbite). Most specimens also contain some orthoclase ($KAlSi_3O_8$). Specimens are usually classified according to the anorthite content (% An) together with the structural type which is deduced from the X-ray diffraction pattern. There are four structural types: (1) the high albite structure $C\bar{1}$, with a-reflections ($h + k = 2n$, $l = 2n$) only, (2) the body-centred structure $I\bar{1}$, with a- and b-relfections ($h + k = 2n + 1$, $l = 2n + 1$), (3) the primitive structure $P\bar{1}$ with a-, b-, c- ($h + k = 2n$, $l = 2n + 1$) and d-reflections ($h + k = 2n + 1$, $l = 2n$), (4) the superlattice structure which appears to be based on a sublattice of the type $I\bar{1}$ and therefore designated $I\bar{1}^*$ [9]. This superlattice gives rise to pairs of e-reflections in place of b-reflections, and f-reflections as satellites to the a-reflections.

Ideally, any particular crystal would exhibit a single structural type which, in general, is dependent upon its An content and its thermal history. However, most real crystals consist of a complex microstructure based on these structural types.

On cooling from the melt, pure anorthite undergoes the transformations $C\bar{1} \rightarrow I\bar{1} \rightarrow P\bar{1}$ in which there is progressive ordering of the Si and Al on the T sites. Consideration of these structures [9] shows that, at each transformation, antiphase domain boundaries may be produced.

The number of stable dislocation Burgers vectors for a given structure is restricted by the requirements that (1) the Burgers vector of a perfect dislocation is a lattice vector and (2) a stable dislocation must not be able to lower its energy by dissociating into two or more dislocations. Since the energy of a dislocation in an isotropic medium is proportional to $\boldsymbol{b}^2$, a dislocation with Burgers vector $\boldsymbol{b}_1$ is unstable if two lattice vectors $\boldsymbol{b}_2$ and $\boldsymbol{b}_3$ exist such that $\boldsymbol{b}_1 = \boldsymbol{b}_2 + \boldsymbol{b}_3$ and $b_1^2 > b_2^2 + b_3^2$ (i.e. the angle θ between $\boldsymbol{b}_1$ and $\boldsymbol{b}_2$ is less than 90°). This restricts the number of Burgers vectors in an approximately isotropic triclinic system to 7. The effects of anisotropy are difficult to estimate since an explicit relation for dislocation energy cannot be written, but it could result in the dislocation being stable when θ is less than, but close to, 90°. The stable Burgers vectors, determined by finding the three shortest non-coplanar lattice vectors **a**, **b** and **c** and finding which of $\mathbf{a} \pm \mathbf{b}$, $\mathbf{b} \pm \mathbf{c}$, $\mathbf{a} \pm \mathbf{c}$ and $\mathbf{a} \pm \mathbf{b} \pm \mathbf{c}$ satisfy the above conditions, are shown in Table I for the three structures $C\bar{1}$, $I\bar{1}$ and $P\bar{1}$. Also included are the unstable Burgers vectors for which the angle θ is close to 90°.

A perfect dislocation $\boldsymbol{b}_1$ can also dissociate into partial dislocations $\boldsymbol{b}_2'$, $\boldsymbol{b}_3'$ connected by a plane of stacking fault if the energy of $\boldsymbol{b}_1$ is larger than the sum of the energies of $\boldsymbol{b}_2'$, $\boldsymbol{b}_3'$ and of the stacking fault. There are no obvious low-energy stacking faults in the $C\bar{1}$ structure so partial dislocations are not expected. However, as a result of the structural transformations $C\bar{1} \rightarrow I\bar{1} \rightarrow P\bar{1}$, low-energy stacking faults associated with b-, c- and d-reflections are available in the $I\bar{1}$ and $P\bar{1}$ structures. All the Burgers vectors listed under these structures in Table I (except [1 0 0], $\frac{1}{2}$[1 1 1] and $\frac{1}{2}$[1 $\bar{1}$ 1]) could dissociate into two partial dislocations with Burgers vectors from those listed under the $C\bar{1}$ structure and connected by a plane of stacking fault. If dissociation occurs, then the stacking fault would be observable with b-, c- and d-reflections but not with a-reflections. The two partial dislocations would be observable with a-reflections providing their separation is greater than the resolution of weak-beam images (about 50 Å). However, if their separation is less than this value they could be inferred only by detailed comparison with computed electron micrographs [10].

TABLE I Posssible Burgers vectors for plagioclase structures

$C\bar{1}$		$I\bar{1}$		$P\bar{1}$	
$\boldsymbol{b}$	$\lvert\boldsymbol{b}\rvert$(Å)	$\boldsymbol{b}$	$\lvert\boldsymbol{b}\rvert$(Å)	$\boldsymbol{b}$	$\lvert\boldsymbol{b}\rvert$(Å)
$\frac{1}{2}$[0 0 1]	7	[1 0 0]	8	[1 0 0]	8
$\frac{1}{2}$[1 $\bar{1}$ 0]	7	$\frac{1}{2}$[1 1 1]	9	[0 1 0]	13
$\frac{1}{2}$[1 1 0]	7	$\frac{1}{2}$[1 $\bar{1}$ 1]	9	[0 0 1]	14
$\frac{1}{2}$[1 $\bar{1}$ 1]	9	$\frac{1}{2}$[$\bar{1}$ 1 1]	12	[1 1 0]	15
$\frac{1}{2}$[1 1 1]	9	$\frac{1}{2}$[$\bar{1}$ $\bar{1}$ 1]1	12	[1 0 1]	12
[1 0 0]	8	[0 0 1]	14	[0 1 1]	19
[2 0 1]	8	[1 0 1]	12	[1 1 1]	18
		[0 1 0]	13		
$\frac{1}{2}$[$\bar{1}$ 1 1]*	12 79°	[1 1 0]*	15 87°		
		[1 $\bar{1}$ 0]*	15 85°	[1 $\bar{1}$ 0]*	15 89°
				[0 1 $\bar{1}$]*	19 87°
				[1 $\bar{1}$ 1]*	18 86°

* These Burgers vectors are unstable according to isotropic criteria, but the angle θ is close to 90°.

If a dissociated dislocation is glissile, then the Burgers vectors of both partial dislocations must lie in the slip plane. Therefore, the possibility of dissociation of a dislocation into partial dislocations separated by less than 50 Å can be discounted if it can be shown that the dislocation is glissile and that either of the possible partial dislocation Burgers vectors does not lie in the slip plane.

Burgers vectors of dislocations in elastically isotropic materials can be directly determined in the electron microscope by use of the invisibility criteria $\mathbf{g}\cdot\boldsymbol{b}=0$ and $\mathbf{g}\cdot\boldsymbol{b}\times\mathbf{u}=0$. Although the elastic anisotropy of the plagioclase feldspars is not high, the use of these criteria here can be misleading unless supported by direct comparison of the observed dislocation images with those produced by computer simulation [10] or by other information.

Nevertheless, in many cases, Burgers vectors can be identified indirectly or the number of possibilities can be reduced. For example, since no more than three of the Burgers vectors listed in Table I are co-planar, knowledge of the slip plane reduces the number of possibilities to three or less. It will be shown below that planar faults associated with the dislocations define their slip planes and in favourable cases a unique determination of the Burgers vector is possible. Additional information can be obtained from the direction of the resolved shear stress if the stress distribution is known to be uniform.

3. Experimental methods and specimen details

The specimens listed in Table II were experimentally deformed to about 5% shortening at a temperature of 800° C with a confining pressure of 10 to 15 kbar and at a strain-rate of $\sim 10^{-5}\,\mathrm{sec}^{-1}$. They were in the form of right circular cylinders 6 to 10 mm long and with length-to-width ratios $\geqslant 2$. The specimens fall into two groups:

(1) The Borg–Heard group. This comprises three specimens (An_1, An_{38} and An_{77}) deformed by Borg and Heard [1, 2]. Transmission electron microscope observations showed: An_{77} is $I\bar{1}$ structure with antiphase domains; An_{38} consists of domains of $I\bar{1}$* structure in a matrix of $C\bar{1}$ structure; An_1 is the $C\bar{1}$ structure.

(2) The Hogarth Range specimen (An_{50}) which was a sample deformed by Christie and Willaime. Electron microscope observations showed that it has the $C\bar{1}$ structure.

Thin sections of the deformed specimens, cut parallel to the cylinder axis, were thinned by ion-bombardment and examined in a JEM 200A electron microscope operating at 200 kV.

4. Observations

4.1. General description of dislocation substructures

In one specimen (An_{50}) a range of dislocation substructures was correlated with varying amounts of strain. Most of the strain was accommodated by a large fracture which traversed the specimen at about 45° to the compression axis. Near the fracture plastic strain was evident optically and the degree of strain decreased as the distance from the fracture increased.

The most heavily deformed areas were com-

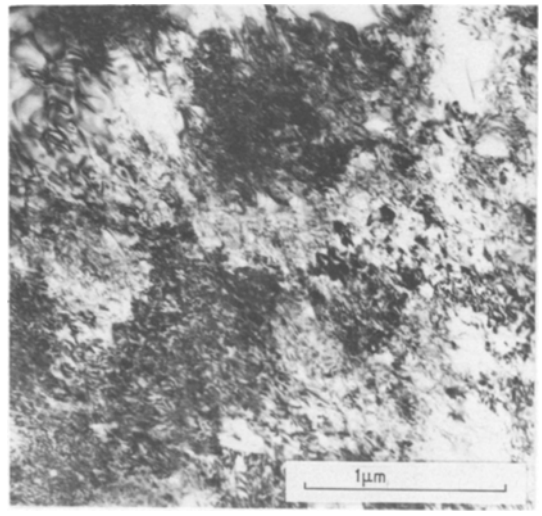

Figure 1 Misoriented domains of tangled dislocations in the most heavily deformed regions of specimen An_{50}. Dark-field image with $\mathbf{g}=(0\,0\,4)$.

TABLE II Details of experimentally deformed specimens

Specimen	Composition*			Origin	Structural state	Deformation conditions
	An	Ab	Or			
An_1	1.0	98.3	0.7	Greenwood, Maine	$C\bar{1}$	800° C 10 kbar, $2\times10^{-5}\,\mathrm{sec}^{-1}$
An_{38}	38.0	61.0	1.0	Sannidal, Norway	$C\bar{1}$ and $I\bar{1}$*	
An_{77}	76.9	22.7	0.4	Crystal Bay, Minnesota – Coarse-grained gabbro	$I\bar{1}$	
An_{50}	50.1	47.5	2.4	Hogarth Range, N.S.W. Phenocrysts from basalt	$C\bar{1}$	800° C, 15 kbar, $10^{-5}\,\mathrm{sec}^{-1}$

* The composition is given by the mol % anorthite (An) albite (Ab) and orthoclase (Or).

posed of irregularly shaped domains (1 to 5 μm across) of tangled dislocations with densities up to 10^{11} cm^{-2}. Examples are shown in Fig. 1. The dislocation density varied between domains by a factor of about 2, and the domains were misoriented by up to 0.5°. Fig. 2a shows the dislocation substructure typically observed within the domains. It will be seen that there are two intersecting sets of dislocations which indicates that two slip systems (at least) are operating in this area of the specimen. This will be discussed in more detail in Section 4.4.

In the less heavily deformed areas, the tangled dislocations are arranged in walls whose orientation is about 15° from (0 0 1). Examples are shown in Fig. 3a. In other regions there is a second set of walls whose orientation is about 15° from (1 0 $\bar{1}$),

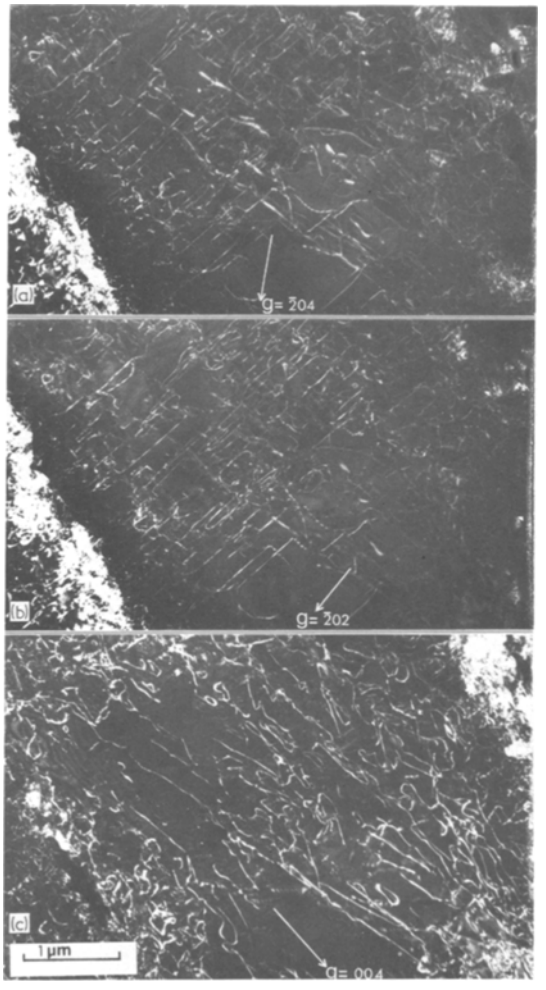

Figure 2 Dark-field images of dislocations in the same area of specimen An_{50}. (a) g = ($\bar{2}$ 0 4), (b) g = ($\bar{2}$ 0 2), (c) g = (0 0 4).

as shown in Fig. 3b. Across these walls there is usually a misorientation of about 0.5°. These walls are similar to the walls of the tangled dislocations that develop approximately parallel to the slip planes in experimentally deformed synthetic quartz [11, 12].

At distances greater than about 1 mm from the main fracture, the dislocation density decreases and the dislocations tend to be in isolated regions. In the centres of these regions there are dense tangles of dislocations, but on the margins the dislocation density is lower and the dislocations are straight. Many pairs of straight dislocations were shown to be dipoles on the basis of the following observations: (1) the strong beam images are related by 180° rotation, implying that the Burgers vectors are opposite, and (2) the relative displacements of the dislocations in weak beam images indicate that their Burgers vectors are opposite. Thus the dislocation substructure may be correlated with the degree of plastic strain. Increasing strain changes the dislocation substructure from isolated regions of dislocations, to walls of dislocations, to domains of high density tangled dislocations with varying dislocation density between the domains.

In areas where the dislocation density was low enough for the strong beam images of the dislocations not to overlap, planar faults were found to be associated with the dislocations. Two different kinds of fault were identified. They are discussed in detail in Sections 4.2 and 4.3.

4.2. Slip-plane faults

Fig. 4a and b show examples of the very faint fringe patterns associated with dislocations in An_{38} and An_{50}. The fringe contrast, although variable from one specimen to another, is weak under all diffracting conditions. However, the contrast is maximum in dark-field when $s \approx 0$, where s is the deviation from the exact Bragg angle. Often the fringes cannot be discerned on the screen of the electron microscope and careful examination of the photographic plate is necessary to detect their presence.

Faults showing similar contrast have been observed by Clarebrough [13, 14] in Cu–Al, Ni–Al and Cu–Zn. He showed, by comparison with computed images, that the fringes were due to a dilation across the fault plane of between 1/150 ⟨1 1 1⟩ and 1/200 ⟨1 1 1⟩. He proposed that this was caused by destruction of short range order.

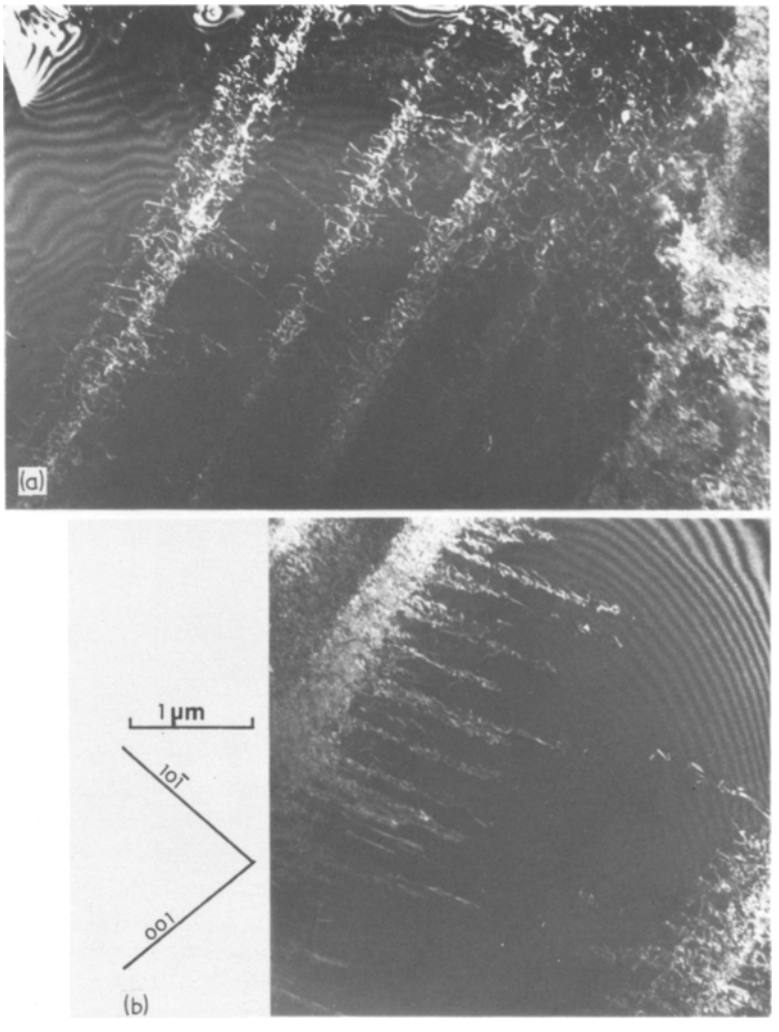

Figure 3 Walls of tangled dislocations in specimen An_{50}, imaged in dark-field with $\mathbf{g} = (0\,0\,4)$ under weak-beam conditions ($s = 0.004$). In (a) the walls are oriented about 15° from (0 0 1). In (b) there is a second set of walls oriented about 15° from (1 0 $\bar{1}$).

Detailed examination of the fringe contrast here indicates that the fringes are out of contrast for reflecting planes that are normal to the fault plane and in contrast, although weak, for all other reflecting planes. This implies that the fault vector is normal to the fault plane and the fault is either due to the dilation or compression across the fault plane. The contrast of the fringes is similar to that observed by Clarebrough, so the magnitude of the dilation or compression is probably similar.

The faults are not produced by a structural transformation (see Section 5) and must, therefore, be produced by the movement of the dislocations. Regardless of the detailed mechanism of their formation they are potentially useful for the determination of slip planes and will be called "slip-plane faults". Furthermore, they indicate the sense of movement of the dislocation on the slip plane and, therefore, can be used to determine the relative sign of the Burgers vector.

4.3. $1/x$ [0 1 0] faults

Examples of the second kind of fault associated with the dislocations in specimens An_1 and An_{38} are shown in Fig. 5a and b, respectively. In An_1 (and An_{77}) the faults are on (1 0 $\bar{1}$) and in An_{38} they are on (1 0 2). Dark-field images of all these faults show the following characteristics: (1) the faults are out of contrast for all reflections of the type $\mathbf{g} = (h0l)$. Application of the visibility criterion $\mathbf{g} \cdot \mathbf{R} = n$ implies that the fault vector is of the form $\mathbf{R} = [0v0]$; (2) the fringes are in contrast for all (hkl) reflections with $k \neq 0$. This was tested for k up to 14 in An_{38} and for k up to 10 in An_1. The

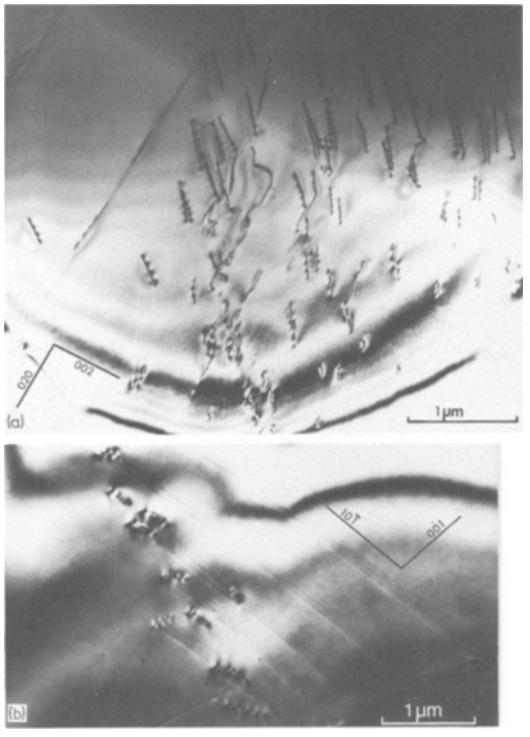

Figure 4 (a) Slip-plane faults in specimen An_{38} imaged in bright-field with the (00*l*) row of systematic reflections operating. (b) Slip-plane faults in specimen An_{50} imaged in dark-field with $\mathbf{g} = (20\bar{2})$ at $s = 0$.

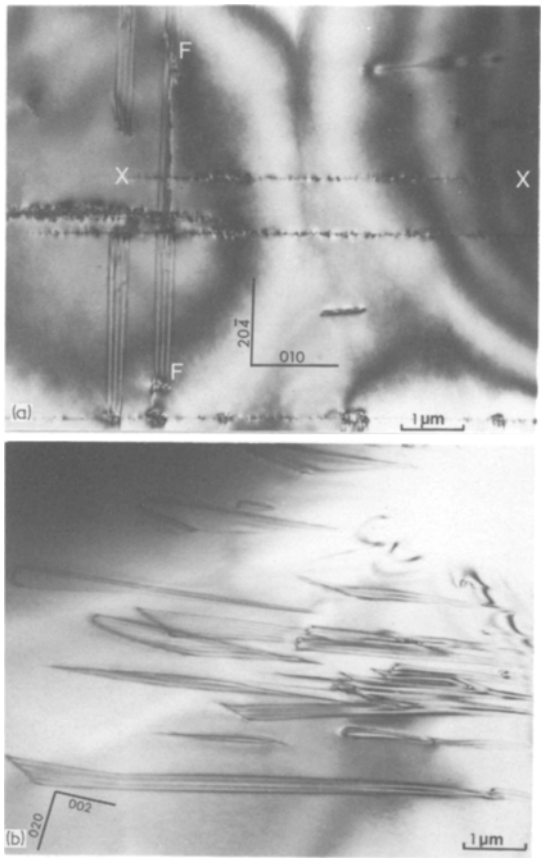

Figure 5 (a) $1/x$ [0 1 0] faults F and microfractures X in specimen An_1. Bright-field image. (b) $1/x$ [0 1 0] faults in specimen An_{38} imaged in bright-field with the (0*k*0) row of systematic reflections operating.

fault vector is, therefore, of the form $\mathbf{R} = 1/x$ [0 1 0] where x is not an integer. $\mathbf{R}$ is parallel to the plane of the faults in all cases.

4.4. Dislocation contrast

Although attempts were not generally made to determine Burgers vectors by application of the invisibility criteria discussed in Section 2, two examples of complete (or almost complete) invisibility were found in An_{50}. These are shown in Fig. 2a to c where the electron beam is almost normal to (0 1 0). Fig. 2a shows that with $\mathbf{g} = (\bar{2}\,0\,4)$ there are two intersecting sets of dislocations which are aligned parallel to the traces of (0 0 1) and $(1\,0\,\bar{1})$. It follows that the dislocations are aligned parallel to $\mathbf{u}_1 = [1\,0\,0]$ and $\mathbf{u}_2 = [1\,0\,1]$, respectively. In Fig. 2b it will be seen that with $\mathbf{g} = (\bar{2}\,0\,2)$ the dislocations aligned parallel to [1 0 0] are in strong contrast, whereas the dislocations aligned parallel to [1 0 1] show only weak residual contrast. For $\mathbf{g} = (0\,0\,4)$ the dislocations parallel to [1 0 0] are completely out of contrast, while those parallel to [1 0 1] are in strong contrast, as shown in Fig. 2c. Head *et al.* [10] considered the conditions under which *complete* invisibility of dislocations in anisotropic media can occur. They found that if the dislocation line is parallel to an even-fold axis of the crystal or normal to a mirror plane then the isotropic invisibility critera apply. Furthermore, there are other special cases where invisibility occurs for dislocations that are not necessarily pure edge or pure screw. However, in all cases where invisibility does occur, both $\mathbf{g} \cdot \boldsymbol{b}$ and $\mathbf{g} \cdot \boldsymbol{b} \times \mathbf{u}$ are zero. These are, therefore, necessary, but not sufficient, conditions for zero contrast.

Of the possible Burgers vectors listed in Table I for the $C\bar{1}$ structure only $\boldsymbol{b} = [1\,0\,0]$ satisfies the invisibility criteria for $\mathbf{g} = (0\,0\,4)$ and $\mathbf{u}_1 = [1\,0\,0]$. $\mathbf{u}_1$ is also a pseudo-tetrad axis. This suggests that the dislocations aligned parallel to [1 0 0] are pure screw. The most likely slip planes are (0 0 1) and (0 1 0). Since for An_{50} there was zero resolved shear-stress on (0 1 0), but high resolved shear-stress on (0 0 1), it must be concluded tentatively

that the slip system of these dislocations is (0 0 1) [1 0 0]. However, a definite identification would require the use of computed images [10].

For the dislocations aligned parallel to [1 0 1] the slip plane must be of the type $(hk\bar{h})$. Of the Burgers vectors listed in Table I for the $C\bar{1}$ structure only $\frac{1}{2}$ [1 $\bar{1}$ 1] and $\frac{1}{2}$ [1 1 1] satisfy $\mathbf{g} \cdot \boldsymbol{b} = 0$ (but *not* $\mathbf{g} \cdot \boldsymbol{b} \times \mathbf{u} = 0$) for $\mathbf{g} = (\bar{2}\,0\,2)$ and $\mathbf{u} = \mathbf{u}_2 = [1\,0\,1]$. Both these Burgers vectors require the slip plane to be $(h\,0\,\bar{h})$ so that the simplest slip system could be (1 0 $\bar{1}$) $\frac{1}{2}$ [1 $\bar{1}$ 1] or (1 0 $\bar{1}$) $\frac{1}{2}$ [1 1 1]. However, these speculations clearly require further evidence to justify them (see Section 5.4).

5. Determination of slip systems using planar faults

A planar fault which is bounded by a dislocation can be produced by (1) the movement of the dislocation (in which case it defines the slip plane), or (2) the movement of the interface of a structural transformation past a dislocation (for example, if a dislocation in the $C\bar{1}$ structure has a Burgers vector which is a lattice vector of $C\bar{1}$ but not of $I\bar{1}$, the transformation $C\bar{1} \rightarrow I\bar{1}$ will produce an antiphase boundary which ends on the dislocation but does not define the slip plane). The only faults that are produced by structural transformations in plagioclase are those associated with *b*-, *c*-, and *d*-reflections. These faults will be out of contrast in dark-field images from *a*-relfections. Therefore, any faults associated with dislocations and observed with *a*-reflections must be a result of movement of the dislocation and, regardless of the detailed mechanism of their formation, they should define the slip plane. In this section identification of slip planes from the faults described in Sections 4.2 and 4.3 is used in conjunction with Table I to determine the slip systems of the dislocations.

5.1. Specimen An_1

This specimen was a single crystal which contained large growth albite twins. The direction of the applied stress relative to the crystallographic axes was, therefore, different within the two twin individuals; it favoured mechanical albite and pericline twinning within one twin and opposed it in the other. The planar faults to be discussed here were only in the latter twin so their development is sensitive to the direction of the applied stress. The plane of the faults is (1 0 $\bar{1}$) and dark-field images show the characteristics of 1/*x* [0 1 0] faults. They are often bounded at both ends by microfractures but many are bounded at one or both ends by dislocations (Fig. 5a).

Since the plane of the faults is (1 0 $\bar{1}$) the slip plane of the dislocations bounding the faults is (1 0 $\bar{1}$). Of the Burgers vectors in Table I only $\boldsymbol{b}_1 = \frac{1}{2}$ [1 1 1] and $\boldsymbol{b}_2 = \frac{1}{2}$ [1 $\bar{1}$ 1] are parallel to (1 0 $\bar{1}$). The Schmidt factor for $\boldsymbol{b}_2$ is 0.49 and for $\boldsymbol{b}_1$ it is zero. Since the faults occur only in one twin and are widely distributed throughout that twin, it appears that the dislocation movement was produced by the applied shear stress rather than local inhomogeneity of the stress field. If this is the case, the Burgers vector is $\boldsymbol{b}_2 = \frac{1}{2}$ [1 $\bar{1}$ 1].

5.2. Specimen An_{38}

Most of the dislocations in An_{38} are associated with slip-plane faults which are curved and vary between ($\bar{1}$ 3 0) and ($\bar{1}$ 2 0) as can be seen in Fig. 4a. Since they are not perfectly planar, cross slip of the dislocations must have occurred. The only Burgers vector in Table I that is parallel to the surface of the faults is $\frac{1}{2}$ [0 0 1] which is parallel to both ($\bar{1}$ 3 0) and ($\bar{1}$ 2 0). The slip systems ($\bar{1}$ 3 0) $\frac{1}{2}$ [0 0 1] and ($\bar{1}$ 2 0) $\frac{1}{2}$ [0 0 1] both have high resolved shear stress, with Schmidt factors of 0.50 and 0.49, respectively.

In several isolated areas, 1/*x* [0 1 0] faults were found to be parallel to (1 0 2). The only Burgers vector possible for this slip plane is [0 1 0] which, from the structural considerations of Section 2, should not be stable in the *C*1 structure. However, this specimen contains domains of $I\bar{1}$* structure, which is based on the $I\bar{1}$ structure and in which [0 1 0] is a stable Burgers vector.

5.3. Specimen An_{77}

This specimen was polycrystalline and has the $I\bar{1}$ structure. Observations of planar faults in two grains have been selected for discussion.

The first grain occupied about half of the specimen and contained slip plane faults on (1 1 $\bar{2}$), (1 3 $\bar{2}$) and (0 1 0), with (1 1 $\bar{2}$) being the most common. Table III shows the possible Burgers vectors for these slip planes, together with Schmidt factors for the applied stress.

Dark-field images from *b*-reflections indicate that antiphase boundaries are associated with most of the (1 1 $\bar{2}$) slip planes and a few of the (1 3 $\bar{2}$) and (0 1 0) slip planes. However, most of the (1 3 $\bar{2}$) and (0 1 0) slip planes do not show antiphase

TABLE III

Slip plane	Possible Burgers vectors	Schmidt factors
$(1\,1\,\bar{2})$	$\frac{1}{2}[2\,0\,1]$	0.50
	$\frac{1}{2}[1\,\bar{1}\,0]$	0.25
	$\frac{1}{2}[1\,1\,1]$	0.25
$(1\,3\,\bar{2})$	$\frac{1}{2}[2\,0\,1]$	0.43
	$\frac{1}{2}[\bar{1}\,1\,1]$	0.32
$(0\,1\,0)$	$\frac{1}{2}[2\,0\,1]$	0.20
	$[1\,0\,0]$	0.32
	$\frac{1}{2}[0\,0\,1]$	0.16
	$[1\,0\,1]$	0.05

boundaries. The faults have been interpreted as slip-plane faults rather than the result of growth of $I\bar{1}$ domains during the $C\bar{1} \rightarrow I\bar{1}$ transformation of a crystal containing dislocations because (1) the faults show the weak contrast from a-reflections which is characteristic of slip-plane faults, whereas perfect antiphase boundaries show no contrast, and (2) the trace of the faults is parallel to $[2\,0\,1]$ throughout the grain, an area much larger than the size of b-domains*.

All the slip planes are parallel to $[2\,0\,1]$, suggesting that $\boldsymbol{b} = \frac{1}{2}[2\,0\,1]$ is a common Burgers vector. However, other Burgers vectors must be involved since dislocations with $\boldsymbol{b} = \frac{1}{2}[2\,0\,1]$ require an antiphase boundary across the slip plane and not all slip planes are associated with an antiphase boundary. The following slip systems are consistent with the above observations and the Schmidt factors calculated from the direction of the applied stress: $(1\,1\,\bar{2})\frac{1}{2}[2\,0\,1]$, $(1\,3\,\bar{2})\frac{1}{2}[2\,0\,1]$ and $(0\,1\,0)\frac{1}{2}[2\,0\,1]$ for the slip planes associated with antiphase boundaries, and $(1\,3\,\bar{2})\frac{1}{2}[\bar{1}\,1\,1]$ and $(0\,1\,0)[1\,0\,0]$ for the slip planes not associated with antiphase boundaries.

The second grain contains fine-scale albite and pericline twins inclined at an angle of 70° to the foil and dislocations in an average density of about 10^8 cm^{-2}. In the area with pericline twinning, the dislocations are generally arranged in low-angle boundaires parallel to the pericline twin plane within one twin orientation but not in the other. This is shown in Fig. 6, where the twin orientations are labelled A and B, respectively.

Faults with the low-contrast characteristic of slip plane faults lead up to, and terminate at, the dislocations in twin A. These slip plane faults are parallel to $(1\,0\,\bar{1})$. This plane is common to both twin individuals since the twin axis is $[0\,1\,0]$. It can be seen in Fig. 6 that the faults are continuous

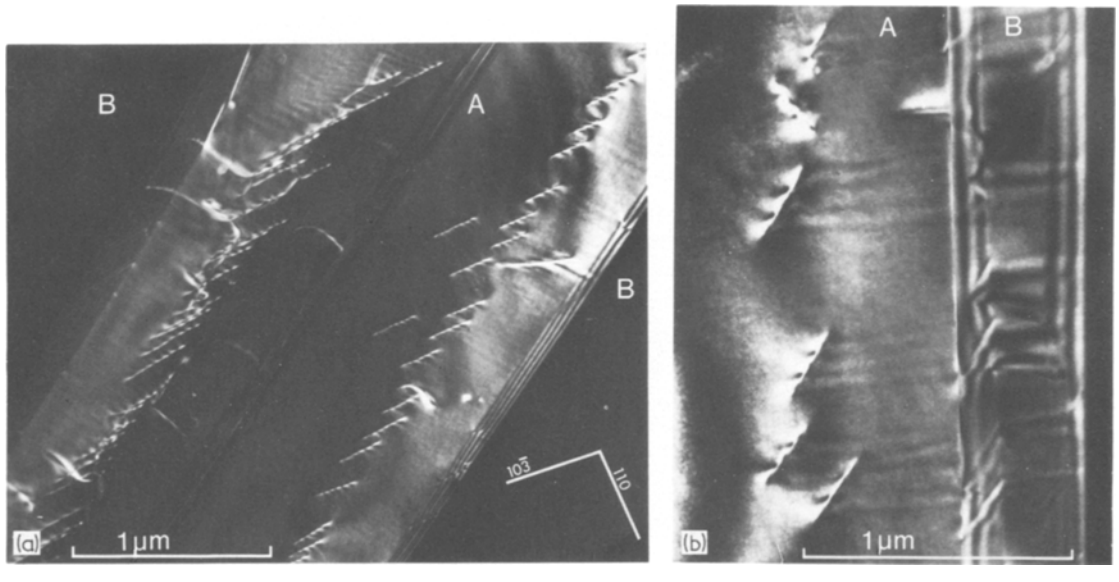

Figure 6 (a) Arrays of dislocations forming low-angle boundaries which are parallel to pericline twin boundaries in Specimen An_{77}. Dark-field image with $\mathbf{g} = (2\,2\,0)$. (b) This is a composite of two micrographs A and B corresponding to the two pericline twin individuals. The micrographs are joined along the twin boundary. In A $\mathbf{g} = (2\,2\,0)$ and in B $\mathbf{g} = (2\,\bar{2}\,0)$. The faults associated with the dislocations in A are continuous across the twin boundary. The fringe contrast is higher in B than in A. However, this contrast difference is greater than shown because A was printed on a more contrasty grade of paper in order to make the fringes in A more clearly observable.

* A b-domain is a region bounded by an antiphase domain boundary which is imaged in dark-field with a **b**-reflection [19].

across the twin boundary except where they terminate on a dislocation that lies on or close to the boundary. However, within twin B they show higher contrast. In fact they show the contrast characteristic of $1/x$ [0 1 0] faults. Therefore, the faults change their nature on passing through the twin boundary.

Within twin A the fault contrast is low for both a- and b-reflections, so the Burgers vector of the dislocations is a lattice vector of the $I\bar{1}$ structure. Since the slip plane of the dislocations is $(1\,0\,\bar{1})$ the possible Burgers vectors from Table I are [0 1 0], [1 0 1], $\frac{1}{2}$ [1 1 1] and $\frac{1}{2}$ [1 $\bar{1}$ 1]. However, the dislocation direction is [0 1 0], so if the Burgers vector is [0 1 0] the dislocations are screw. Since it is impossible to form a low-angle boundary free of long range stresses with a single set of screw dislocations [15], this Burgers vector can be eliminated. Ideally, such a boundary should consist of a set of pure edge dislocations with the Burgers vector normal to the boundary. This condition is almost satisfied for $\boldsymbol{b} = [1\,0\,1]$ since [1 0 1] is only 6° from the normal to the boundary (the rhombic section) and the dislocations are only 4° from the pure edge. However, if the Burgers vector is $\frac{1}{2}$ [1 1 1] or $\frac{1}{2}$ [1 $\bar{1}$ 1], the dislocations would be 40° from the edge orientation. Therefore, the Burgers vector $\boldsymbol{b} = [1\,0\,1]$ appears most likely.

Since the slip plane faults are observed to pass through the twin boundary, the interaction of the dislocations with the boundary must be considered. The slip plane, $(1\,0\,\bar{1})$, is unchanged across the boundary but all lattice vectors within the slip plane except [0 1 0] are changed. A dislocation with Burgers vector [0 1 0] could pass unaffected through the boundary, but this is not so for other Burgers vectors. The situation for $\boldsymbol{b} = [1\,0\,1]$ is shown in Fig. 7a. There are two possibilities. Firstly, $\boldsymbol{b} = [1\,0\,1]$ in twin A could be resolved into two components, $b_{\parallel}$ and $b_{\perp}$, parallel and perpendicular to [0 1 0]. Both of these directions are unchanged across the boundary, so both components could pass through the boundary. However, the Burgers vector $\boldsymbol{b}$ is not a lattice vector of twin B, so its propagation requires a fault with fault vector $\mathbf{R} = 2b_{\parallel} = 0.13$ [0 1 0] to be left in the slip plane. Alternatively, the Burgers vector $\boldsymbol{b}$ could dissociate into $\boldsymbol{b}' + 2b_{\parallel}$ leaving $2b_{\parallel}$ in the twin boundary and propagating $\boldsymbol{b}' = [\bar{1}\,0\,\bar{1}]$ which is a lattice vector in twin B.

The observations are consistent with the first of these mechanisms since the faults in twin B were observed to have an associated fault vector of the form $1/x$ [0 1 0] in agreement with the fault vector $\mathbf{R} = 2b_{\parallel} = 0.13$ [0 1 0] calculated above. Furthermore, no dislocation is observed in the twin boundary where the faults cross. However, this observation may not be conclusive because the small Burgers vector (0.13 [0 1 0]) may not give detectable contrast. It is interesting to note that with either mechanism a jog is left in the twin boundary where the dislocation crosses.

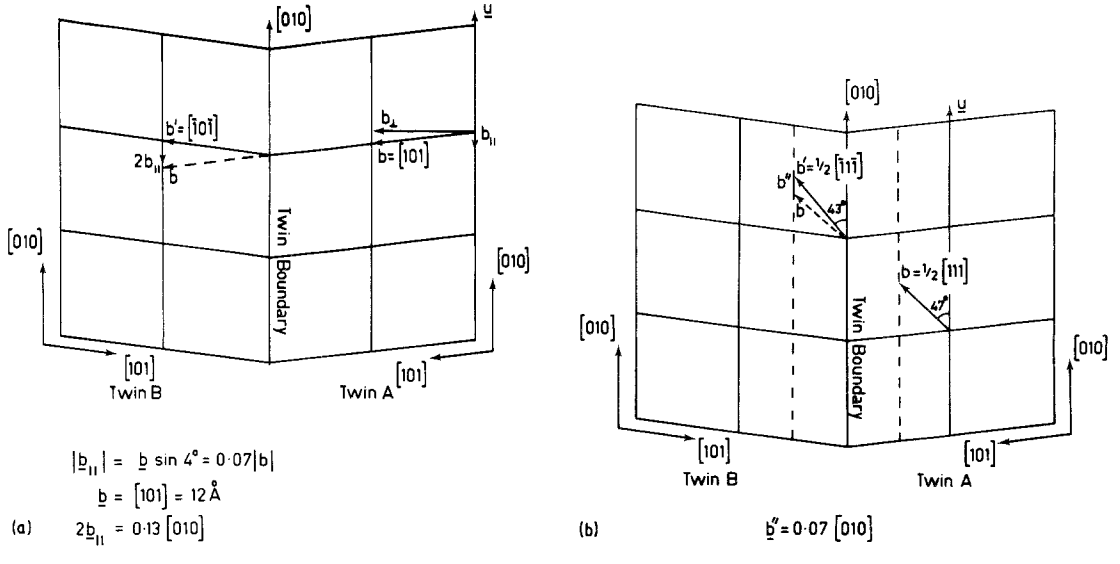

Figure 7 Diagrams showing the interaction of a pericline twin boundary and a dislocation with Burgers vector $\boldsymbol{b}$ and direction $\mathbf{u} = [0\,1\,0]$, when the dislocation passes from twin A into twin B. (a) $\boldsymbol{b} = [1\,0\,1]$, (b) $\boldsymbol{b} = \frac{1}{2}$ [1 1 1]

The mechanism for $\boldsymbol{b} = \frac{1}{2}[1\,1\,1]$ or $\boldsymbol{b} = \frac{1}{2}[1\,\bar{1}\,1]$ is shown in Fig. 7b. The possibilities are the same as for $\boldsymbol{b} = [1\,0\,1]$ except that the fault vector for the first mechanism is $\mathbf{R} = \boldsymbol{b}'' = 0.07\,[0\,1\,0]$, and, for the second mechanism, $\boldsymbol{b} = \frac{1}{2}[1\,1\,1]$ in twin A becomes $\boldsymbol{b}' = [\bar{1}\,1\,\bar{1}]$ in twin B and vice versa.

The Schmidt factors for the applied stress are 0.5 for $(1\,0\,\bar{1})[1\,1\,1]$ and 0.38 for $(1\,0\,\bar{1})[1\,0\,1]$. However, their reliability is doubtful because this grain was a small one and it is likely that the applied stress does not represent the true stress distribution. Both of these slip systems are therefore possible, although $(1\,0\,\bar{1})[1\,0\,1]$ appears to be more likely from considerations of the nature of low-angle boundaries.

5.4. Specimen An_{50}

This specimen contains slip-plane faults which are mostly parallel to $(1\,0\,\bar{1})$. Therefore, the possible Burgers vectors are $\frac{1}{2}[1\,1\,1]$ or $\frac{1}{2}[1\,\bar{1}\,1]$. The directions $[1\,1\,1]$ and $[1\,\bar{1}\,1]$ are structurally pseudo-equivalent (since $[0\,1\,0]$ is a pseudo-diad axis) and the Schmidt factors for the applied stress are equal. Thus both Burgers vectors probably exist. This is in agreement with the considerations of the contrast of dislocations in this specimen (Section 4.4).

5.5. Summary of slip systems

From the observations of dislocations given above it is possible to summarize the observed slip systems. This is done in Table IV.

To this must be added the slip $(0\,0\,1)[1\,0\,0]$ determined from contrast considerations in Section 4.4

TABLE IV

Specimen	Slip plane	Possible Burgers vectors
An_1	$(1\,0\,\bar{1})$	$\frac{1}{2}[1\,1\,1]$
An_{38}	Not planar; varies between $(\bar{1}\,3\,0)$ and $(\bar{1}\,2\,0)$	$\frac{1}{2}[0\,0\,1]$
An_{77} grain 1	$(1\,1\,\bar{2})$	$\frac{1}{2}[2\,0\,1]$
	$(1\,3\,\bar{2})$	$\frac{1}{2}[2\,0\,1]$, $\frac{1}{2}[\bar{1}\,1\,1]$
	$(0\,1\,0)$	$\frac{1}{2}[2\,0\,1]$, $[1\,0\,0]$
grain 2	$(1\,0\,\bar{1})$	$[1\,0\,1]$ or $\frac{1}{2}[1\,1\,1]$ and $\frac{1}{2}[1\,\bar{1}\,1]$
An_{50}	$(1\,0\,\bar{1})$	$\frac{1}{2}[1\,1\,1]$ and/or $\frac{1}{2}[1\,\bar{1}\,1]$

6. Discussion

It is clear from this study that there are many slip systems available in plagioclase feldspars, that cross slip is common and that slip by dislocation motion is a major mechanism of deformation. Therefore, it is important to consider the mechanisms of dislocation generation. In An_{50} they were only produced in areas close to the main fracture where there are also abundant microfractures. This suggests that these fractures are associated with at least the initial production of dislocations. Li [16] has suggested a mechanism of punching half loops of dislocations from ledges of a free surface. In this case the surface ledges would be cleavage steps or ripples commonly observed on fracture surfaces [17]. Evidence for the operation of surface dislocation sources in experimentally deformed quartz has been represented by Morrison-Smith [12]. Also, in this and several other specimens, isolated regions of dislocations were found to be centred on irregularly shaped voids. Near these voids the dislocations are tangled and the dislocation density decreases away from the voids with the dislocations becoming straighter. The slip plane faults of the dislocations all lead back to the areas of tangled dislocations, indicating that the dislocations all originated from that area. This implies that the voids play some role in the generation of dislocations. Similar isolated regions of dislocations are produced by inclusions in quartz [12].

Planar faults appear to be produced by the movement of all dislocations in the plagioclase feldspars and these faults have proved to be useful indicators of slip planes. However, the structures of the faults are not clear. The slip-plane faults involve only a very small displacement normal to the slip plane and Clarebrough [13] has shown that in Cu–Al this can be produced by destruction of short-range order across the slip plane. However, detailed discussion of this mechanism is precluded by the lack of knowledge of the detailed nature of short-range order in plagioclase. Another mechanism which could produce this kind of fault is the imperfect reconstruction of Al/Si–O bonds after the passage of a dislocation. Any displacements parallel to the slip plane would on average cancel, whereas those normal to the slip plane might not.

The $1/x\,[0\,1\,0]$ faults involve a displacement vector $\mathbf{R}$ which is parallel to the plane of the fault

but is not a simple fraction of a lattice vector. Such a fault could be produced either by a simple displacement in the fault plane or the formation of a thin coherent layer of a different structure or a different orientation (twin) which produces relative displacement **R** of the crystal either side of it. It is difficult to envisage how a simple stacking fault of this nature could occur, but one possible mechanism was suggested by the consideration of dislocation interactions with a pericline twin boundary in Section 5.3. There it was found that one way in which a dislocation, on a slip plane common to both twins, could pass through the twin boundary was to continue with the same Burgers vector which is not a lattice vector of the second twin. This requires a fault with $\mathbf{R} = 0.07\ [0\,1\,0]$ or $\mathbf{R} = 0.13\ [0\,1\,0]$ to be left in the slip plane. Faults of this type have been observed in An_{77}. However, pericline twins were not observed in An_1 and only a few narrow deformation pericline twins were found in An_{38}. Furthermore the only Burgers vector possible for An_{38} is $[0\,1\,0]$. This is common to both pericline twin orientations so it would not produce a fault. If the fault is produced by a coherent layer then two possibilities that would give the required displacement parallel to $[0\,1\,0]$ are the monoclinic feldspar structure or a pericline twin. The pericline twin appears to be more likely because this twin is commonly found in these materials, whereas exsolution of the monoclinic structure is never found. The lowest energy interface for pericline twins is the rhombic section [18] but, since it is an axial twin law, it is geometrically possible for any plane parallel to $[0\,1\,0]$ to be a composition plane. Although the planes of the $1/x\ [0\,1\,0]$ faults vary, they are always parallel to $[0\,1\,0]$. A layer of pericline twin would produce a displacement ($R = 2t \tan \theta$) of the lattice either side of it, where t is the thickness of the layer and θ is the obliqueness of the twin.

As already pointed out, slip by dislocation movement is only one of the mechanisms of deformation. The other mechanisms and their interactions with each other and with dislocations will be discussed elsewhere, together with the relevance of these experimental observations to the deformation of feldspars in nature.

Acknowledgements

We thank Drs I. Y. Borg and H. C. Heard for the opportunity of examining their experimentally deformed specimens, Drs J. M. Christie and C. Willaime for experimentally deforming some of our specimens, and the Australian Research Grants Committee for generous financial support.

References

1. I. Y. BORG and H. C. HEARD, *Contr. Mineral. and Petrol.* **23** (1969) 128.
2. *Idem,* "Experimental and Natural Rock Deformation" (Springer Verlag, Berlin, 1970) p. 375.
3. G. W. LORIMER, P. E. CHAMPNESS and E. T. C. SPOONER, *Nature* **P239** (1972) 108.
4. G. W. LORIMER, H. NISSEN and P. E. CHAMPNESS, *Schweiz. Mineral. Petrog. Mitt* **54** (1974) 707.
5. S. WHITE, *Contr. Mineral. and Petrol.* **50** (1975) 289.
6. D. B. MARSHALL and C. J. L. WILSON, *ibid* (1975).
7. J. S. LALLY, R. M. FISHER, J. M. CHRISTIE, D. T. GRIGGS, A. H. HEUER, G. L. NORD and S. V. RADCLIFFE, Proceedings of the Third Lunar Science Conference, Houston, Vol. 1 (1972).
8. J. V. SMITH, "Feldspar Minerals", Vol. 1 (Springer Verlag, Berlin, 1974).
9. A. C. McLAREN and D. B. MARSHALL, *Contr. Mineral. and Petrol.* **44** (1974) 237.
10. A. K. HEAD, P. HUMBLE, L. M. CLAREBROUGH, A. J. MORTON and C. T. FORWARD, "Computed Electron Micrographs and Defect Identification" (North-Holland, Amsterdam, 1973).
11. A. C. McLAREN, R. G. TURNER, J. N. BOLAND and B. E. HOBBS, *Contr. Mineral. and Petrol.* **29** (1970) 104.
12. D. J. MORRISON-SMITH, Ph.D. Thesis, Australian National University, Canberra (1974).
13. L. M. CLAREBROUGH, *Phys. Stat. Sol. (a)* **18** (1973) 427.
14. *Idem, ibid* **32** (1975) K5.
15. J. P. HIRTH and J. LOTHE, "Theory of Dislocations" (McGraw-Hill, New York, 1968).
16. J. C. M. LI, *Trans. Met. Soc. AIME* **227** (1963) 239.
17. J. S. WILLIAMS, B. R. LAWN and M. V. SWAIN, *Phys. Stat. Sol. (a)* **2** (1970) 7.
18. R. W. CAHN, *Adv. Phys.* **3** (1954) 363.

Received 9 September and accepted 4 October 1976.